Volume 1 | Number 1 | Jan 2013 | Pages 1–100

Nanoscale

www.rsc.org/nanoscale

ROYAL SOCIETY OF CHEMISTRY

ROYAL SOCIETY OF CHEMISTRY

www.rsc.org/nanoscale

Journal Name

Dynamic Article Links ▶

ARTICLE TYPE

Synthesis of polybenzoxazine based nitrogen-rich porous carbons for carbon dioxide capture

Liu Wan [a,b], Jianlong Wang [a], Chong Feng [a,b], Yahui Sun [a,b], Kaixi Li [a*]

Nitrogen-rich porous carbons (NPCs) were synthesized from 1,5-dihydroxynaphthalene, urea, and formaldehyde based on benzoxazine chemistry by a soft-templating method with KOH chemical activation. They possess high surface areas of 856.8-1257.8 m^2 g^{-1}, large pore volume of 0.15-0.65 cm^3 g^{-1}, tunable pore structure, high nitrogen content (5.21-5.32 wt. %), and high char yields. The amount of the 10 soft-templating agent F127 has multiple influences on the textural and chemical properties of the carbons, affecting the surface area and pore structure, impacting the compositions of the nitrogen species, and resulting in the improvement of the CO_2 capture performance. At 1 bar, high CO_2 uptakes of 4.02 and 6.35 mmol g^{-1} at 25 and 0 ^{o}C was achieved for sample NPC-2 with the molar ratio of F127 : urea = 0.010 : 1, respectively. It can be attributed to its well-developed micropore structure and abundant pyridinic 15 nitrogen, pyrrolic nitrogen and pyridonic nitrogen functionalities. It also exhibits a remarkable selectivity for CO_2/N_2 separation and fast adsorption / desorption rate and it can be easily regenerated. It suggests that the polybenzoxazine-based NPCs are desirable for CO_2 capture because of possessing high micropore surface area, large micropore volume, appropriate pore size distribution, and a large number of basic nitrogen functionalities.

20 1 Introduction

Recently, developing efficient methods for carbon dioxide capture and sequestration (CCS) have aroused much attentions due to a series of environmental problems, such as global warming issues and rising of sea levels.[1,2] Various technologies 25 including absorption, adsorption, membrane separation, and cryogenic distillation have been widely applied for CO_2 capture.[3,4] The conventional, well-developed amine absorption technology is employed in industry for large-scale CO_2 capture, but it presents several drawbacks, such as low efficiency, high 30 energy requirement, equipment corrosion, and solvent loss.[5,6,7] Adsorption by porous carbons, especially by nitrogen-enriched porous carbons (NPCs), shows great potential to reduce the cost, save energy, and avoid additional environmental problems, which has been considered to a promising technology for high-efficient 35 CO_2 capture.[8,9] The NPCs almost encompass all prerequisite attributes for CO_2 capture: high CO_2 capacity, fast adsorption/desorption rate, short regeneration time and low regeneration temperature due to their high surface area, large pore volume, tunable pore structure, and controllable chemical 40 properties.[10,11]

It has been reported that the incorporation of basic nitrogen functionalities into the carbon network of the porous carbon materials is beneficial for adsorption of acidic CO_2 gas by enhancing the affinity and interaction between CO_2 molecules 45 and the adsorbents.[12,13] The NPCs exhibit higher CO_2 adsorption capacities and better CO_2/N_2 selectivity, in comparison with porous carbons without incorporation of any heteroatoms.

Therefore, preparation of high-performance NPCs in a simple way for CO_2 capture becomes increasingly attractive. Up to now, 50 there are mainly two types of strategies to synthesize the NPCs: one is the indirect way, such as impregnation for anchoring amine groups,[14,15,16,17,18] reaction with nitrogen containing reagents,[19,20] thermal treatment with NH_3 gas[21,22] at high temperature to load nitrogen functional groups; the other is the direct way, mainly by 55 utilizing the nitrogen-rich precursors, including nitrogen-containing organic polymers,[23,24,25] biomass[26,27,28] or biomimetic materials[29] as carbon and nitrogen sources, nitrogen-containing reagents as catalyst[30,31] or additives.[32,33] The direct way is usually preferable due to many advantages of simple procedures, time-60 saving, low cost, controllable nitrogen-doping, well-distributed nitrogen atoms in both surface and main body phase, etc. However, direct methods exhibit several disadvantages, such as less developed porosity, low surface area, and poor thermal stability, and low char yield, which lead to low CO_2 adsorption 65 capacity. Thus, it is highly desirable to develop new nitrogen-rich precursors to synthesize NPCs with large surface area, high nitrogen content, and high char yield via one-step procedure.

Polybenzoxazines (PBZs), a new class of high performance heterocyclic resins, are considered to be one of the promising 70 precursors for the synthesis of nitrogen-rich carbons. They show many advantageous properties, such as molecular design flexibility, excellent thermal stability, high char yield, no need of catalysts or additives, no generation of byproducts, and near-zero shrinkage upon polymerization.[34,35,36] The excellent thermal 75 stability of the PBZ makes it possible to maintain high nitrogen

Nanoscale Accepted Manuscript

content during thermal treatment and high char yield after pyrolysis, due to the presence of stable intramolecular 6-membered-ring hydrogen bonding in the main chain of PBZ.[37] Furthermore, the content and the type of nitrogen functionalities in PBZs can be easily adjusted by changing the type or the proportion of a primary amine or nitrogen containing phenolic compounds, which is attractive for the incorporation of nitrogen atoms into the carbon framework. However, there are only a few reports on the synthesis of porous carbons derived from polybenzoxazines.[38]

It is well-known that phenolic resins can be utilized as carbon presursors to successfully synthesize ordered mesoporous carbon materials by organic-organic self-assembly using triblock copolymers as the soft-templating agent.[39] By comparison, it can be found that phenolic resin and PBZ resins have some similarities. Based on benzoxazine chemistry, benzoxazine monomer contains nitrogen and oxygen containing six-membered heterocyclic group-oxazine ring, similar to the hydroxyl groups in phenolic resins, which is liable to form polymer nanostructures via strong hydrogen bonds. After thermally induced ring-open polymerization, the monomer can be transformed into high performance polymer with a phenolic hydroxyl group and a tertiary amine bridge as a repeating unit.[40] In addition, the existence of stable intramolecular 6-membered-ring hydrogen bonding in the main chain of PBZ might avoid the destruction of the nanostructures. Therefore, it is possible to develop nanostructure in the resultant carbon materials from the PBZs by a soft-templating method.

In this work, we report for the first time the synthesis of PBZ-based NPCs by a soft-templating method in combination with KOH chemical activation. A novel benzoxazine monomer with high thermal stability was firstly prepared from 1,5-dihydroxynaphthalene, urea, and formaldehyde via a solution method. The soft-templating agent F127 was introduced into benzoxazine solution to interact and assemble with the nitrogen and oxygen functionalities in the benzoxazine via hydrogen bonds. Then, the nanostructured resin composites were formed by the evaporation-induced self-assembly strategy (EISA)[38]. After polymerization, carbonization at 600 ^{o}C in N$_2$, and KOH activation at 600 ^{o}C in N$_2$, a series of NPCs with developed porosities and high nitrogen content were obtained. The pore structure of the NPCs can be tailored by changing the concentration of the soft-templating agent F127. The influence of pore structure and surface chemistry of the NPCs on CO$_2$ capture is comprehensively investigated.

Experimental

Materials

1,5-dihydroxynaphthalene (99.9%), urea, formaldehyde (37 wt.% in water), absolute ethanol, hydrochloric acid (36-38 wt.%), and KOH were purchased from Tianjin Tianli Chemical Corp. Poly(ethylene oxide)-poly (propylene oxide)-poly(ethyleneoxide) triblock copolymer (EO$_{106}$PO$_{70}$EO$_{106}$) Pluronic F127 were purchased from BASF Corp. All solvents and other chemicals were AR grade and utilized without further purification.

In a typical preparation, the compositions were for F127 / urea / 1,5-dihydroxynaphthalene / formaldehyde / EtOH = 0.020:1:1:4:32.6 (molar ratio). To a 250 mL three-necked round

bottom flask equipped with a magnetic stirrer, a thermometer, and a reflux condenser, urea (4.0 g), formaldehyde (8.0 g) were added and gradually heated to 90 ^{o}C for 30 min and then cooled to room temperature, denoted as solution A. F127 (16.8 g) and 1,5-dihydroxynaphthalene (10.6 g) were dissolved in absolute ethanol (100.0 g) and stirred for 60 min, denoted as solution B. Then, solution B was added into solution A, and heated under reflux at 90 ^{o}C for 6 h. After cooled to room temperature, the reaction mixture was poured into dishes and to evaporate ethanol at room temperature for 12 h. The obtained benzoxazine monomer together with surfactant F127 mixtures were heated stepwise in an oven at 120, 150, 180, 220, and 260 ℃ for 4 h, respectively. Then, the cured PBZ containing surfactant F127 were further carbonized under a nitrogen atmosphere by heating at 600 ^{o}C for 5 h with a ramp rate of 1 ^{o}C min^{-1}. The obtained carbonized material was denoted as NPC-c (molar ratio of F127 : urea = 0.020 : 1). Subsequently, the carbonized sample was thoroughly mixed in an aqueous KOH solution in a weight ratio of KOH : carbonized sample = 2 : 1, and followed by water evaporation at 120 ^{o}C for 12 h. The activation process was carried out at 600 ^{o}C for 1 h in a tube furnace under flowing nitrogen with a ramp rate of 3 ^{o}C min^{-1}, respectively. The products were repeatedly washed with 1 M HCl and deionized water until the pH value of the filtrate reached about 7 and dried at 110 ^{o}C for 12 h. The resulting activated sample derived from NPC-c was named as NPC-4. By varying the molar ratios of F127 : urea (ranging from 0 : 1, 0.005 : 1, 0.010 : 1, 0.015 : 1 to 0.020 : 1), a series of KOH-activated NPCs were prepared, which were accordingly denoted as NPC-0, NPC-1, NPC-2, NPC-3, and NPC-4, respectively. For comparison, the preparation of sample NPC-2-HCl is as follows: Sample NPC-2 (5.0 g) was added into the concentrated HCl (36-38 wt. %, 50 mL) and stirred adequately for 24 h at room temperature. The HCl treated NPC-2 was then washed with abundant water until the pH of the filtrate was neutral, and further dried at 110 ^{o}C for 12 h.

Material Characterization

N$_2$ adsorption isotherms were measured using a Micromeritics ASAP2020 analyzer at -196 ^{o}C. Before measurements were taken, all samples were degassed at 473 K for 12 h. The specific surface areas (S$_{BET}$) was calculated by the Brunauer–Emmett–Teller (BET) method based on the adsorption data in the relative partial pressure p/p$_0$ range of 0.04 to 0.20. The total pore volume values (V$_{total}$) were estimated from the adsorbed amount at a relative pressure P/P$_0$ of 0.99. The micropore surface area (S$_{micro}$) and micropore volume (V$_{micro}$) were obtained by *t*-plot analysis. The pore size distributions (PSDs) were derived from the density functional theory (DFT) model assuming the split-shaped pores. Scanning electron microscope (SEM) investigations were carried out with a JEOL JSM-700 microscope instrument at an accelerating voltage of 10.0 kV. X-ray photoelectron spectra (XPS) was obtained on a AXIS Ultra DLD spectrometer with an exciting source of MgKα (1486.6 eV). Elemental analysis was performed by an Elementar Vario Macro EL Cube microanalyzer. Fourier transform infrared (FT-IR) spectroscopy was carried out using a Bruker Vertex70 spectrometer over the wavenumber range of 4000-400 cm^{-1}. Thermogravimetric analysis (TGA) curves were recorded on a TA Q500 analyzer from room temperature to 850 ^{o}C with a heating rate of 10 ^{o}C min^{-1} under a

Journal Name

Nanoscale

ARTICLE TYPE

constant nitrogen flow of 50 mL min^{-1}.

CO$_2$ capture measurement

The CO$_2$ and N$_2$ adsorption isotherms were carried out on an automated gas sorption analyzer (Quantachrome Autosorb-1, USA) via conventional volumetric technique at 0 and 25 ^{o}C, respectively. Before the gas adsorption measurement, the sample was evacuated at 150 ^{o}C for at least 6 h. To investigate the recyclability of the NPCs for CO$_2$ capture, the sample was firstly regenerated by evacuating at 150 ^{o}C for 6 h in vacuum, and after that four successive runs of adsorption isotherms were recorded. The adsorption-desorption kinetics of the CO$_2$ and the adsorption-desorption cycles were further measured by a simultaneous TGA analysis using a thermogravimetric analyzer (TGA, Q500, TA instruments, USA) at ambient pressure. In a typical experiment, about 10 mg of the samples were dried at 150 ^{o}C for 2 h under a 50 ml min^{-1} flow of N$_2$ to remove moisture and other remaining molecules. Then, the temperature was decreased to 25 ^{o}C under N$_2$ flow. Subsequently, N$_2$ was changed to 100 % CO$_2$ with a flow rate of 50 ml min^{-1} and the adsorption process was held isothermally for 60 min. The gas was switched back from CO$_2$ to N$_2$. Then, the sample was heated to 100 ^{o}C and was held for 60 min for the desorption of CO$_2$. The same temperature procedure was carried out with a gas mixture composed of 15 % CO$_2$ in nitrogen. The CO$_2$ uptake of the samples was also tested at 75 ^{o}C by a TGA analysis.

Results and discussion
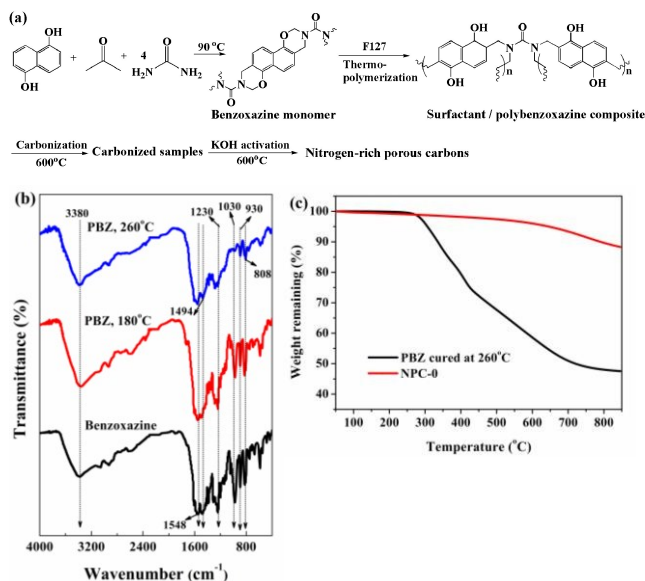
Fig. 1 (a) Chemical reaction of the monomer synthesis, thermally activated ring-opening polymerization and formation of the NPCs, (b) FT-IR spectra of the benzoxazine, PBZ cured at 180 and 260 ^{o}C, respectively, (c) TG curves of the PBZ cured at 260 ^{o}C and NPC-0 under nitrogen atmosphere.

In order to obtain the NPCs with high nitrogen content and good thermal stability, a novel multifunctional main-chain benzoxazine monomer was firstly synthesized from a difuctional phenol (1,5-dihydroxynaphthalene), a difuctional amine (urea), and formaldehyde via a solution method. The synthesis reaction mechanism and thermally activated ring-opening polymerization reaction are shown in Fig. 1. The benzoxazine monomer, PBZs cured at 180 and 260 ^{o}C were characterized by FT-IR spectroscopy (Fig. 1b). The broad peaks at about 3380 cm^{-1} for the monomer, PBZ cured at 180 and 260 ^{o}C belong to the O-H or N-H stretching mode of the phenolic hydroxyl group and amine group. The characteristic peaks at 930 cm^{-1} (out of plane-bending vibrations of C-H), 1230 cm^{-1} (asymmetric stretching of C-O-C), 1030 cm^{-1} (symmetric stretching of C-O-C), 1081 cm^{-1} (asymmetric stretching of C-N-C), 1340 cm^{-1} (CH$_2$ wagging), and 1470-1600 cm^{-1} (benzene ring) correspond to benzoxazine structure, respectively.[31] It confirms the successful synthesis of a new benzoxazine. These characteristic absorption peaks gradually decreased with the increase of curing temperature from 180 to 260 ^{o}C, indicating the increase of the extent of the ring-opening of the monomer at higher temperature. In addition, the absorption intensity of O-H or N-H at 3380 cm^{-1} increased evidently with the increase of curing temperature, owing to the formation of more O-H group through oxazine ring-opening reaction. It implies that benzoxazine monomer could take place thermally activated ring-opening polymerization reaction to form PBZs at 180-260 ^{o}C.

TGA was used to investigate the carbonization process and mechanism of the PBZ cured at 260 ^{o}C in nitrogen atmosphere. As shown in Fig. 1c, no obvious weight loss (4.0 wt. %) below 300 ^{o}C was observed in the TG curve of the PBZ, due to its low water absorption property. The highest weight loss of around 37.4 wt. % during heat treatment in the range of 300-600 ^{o}C is due to the framework carbonization and the decomposition of nitrogen species. The third weight loss of 11.0 wt. % above 600 ^{o}C is due to further release of carbon containing and nitrogen containing gaseous products. At the end, approximately 47.5 wt. % of carbon residues were left at 850 ^{o}C. The TG curve of NPC-0 displays a negligible weight loss at 100-400 ^{o}C, and gradual weight loss of 8.5 wt. % occurs between 400 and 800 ^{o}C. Moreover, the char yield and the nitrogen content of NPC-0 retained as high as 58.4 % and 5.32 wt. % (see Table 1 and Table S1†), respectively, exhibiting outstanding thermal stability. It can be attributed to the existence of the fused rings in the PBZ with rigid polymeric framework, which further extended the 2D-framework of the PBZ and improved its cross-linking density. In order to develop mesopores in the carbon materials, a soft-templating agent (surfactant F127) was introduced into the benzoxazine solution to form mesostructured composite via hydrogen bonds between PEO segments of F127 and O, N species of benzoxazines by EISA.[8,38] The mesopores were created after the decomposition of the surfactant F127 at 600 ^{o}C during the carbonization process. Furthermore, KOH activation method was applied to enhance the microporosities of the NPCs.
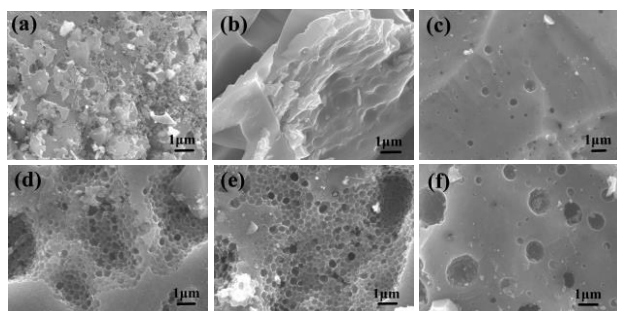
Fig. 2 SEM images of (a) NPC-c, (b) NPC-0, (c) NPC-1, (d) NPC-2, (e) NPC-3, and (f) NPC-4.

5 Fig. 2 shows the SEM images of the NPCs. NPC-c displays the morphology of the aggregates of small, loose carbon particles, which was liable to be activated by KOH (Fig. 2a). No obvious voids or pores were observed on the surface of NPC-0 (Fig. 2b). But NPC-1 has few shallow cavities with sizes of over several
10 hundred nanometers (Fig. 2c). Noticeably, NPC-2 and NPC-3 show abundant spherical cavities on their surfaces (Fig. 2d and 2e), which might result from the release of the residual ethanol solvent gas bubble during the curing process. The size of cavities increased from hundreds of nanometers for NPC-2 and NPC-3 to
15 a few micrometers for NPC-4 (Fig. 2f). This phenomenon can be ascribed to the collaborative effects of the decomposition of the largest amount of surfactant and the chemical activation. The lowest yield for NPC-4 also demonstrates it (Table 1).
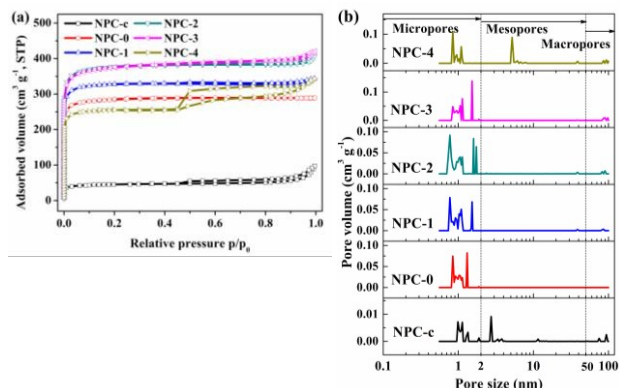
20 **Fig. 3** (a) N_2 adsorption isotherms and (b) DFT pore size distributions for the NPCs.

The textural characteristic of all NPCs was analyzed by N_2 sorption at 77 K. As shown in Fig. 3a, the N_2 sorption isotherm of NPC-c is of type IV with a hysteresis loop, indicating the
25 presence of mesopores. The PSD of NPC-c in Fig. 3b also demonstrates the presence of mesopores in the range of 2.5-2.7 nm. NPC-0~NPC-3 exhibit type I isotherm, with significant nitrogen uptake at relative pressure p/p_0 lower than 0.1, indicating the presence of large amount of micropores. In detail, NPC-0 is a

30 typical microporous carbon material with no mesopores, which is dominated by micropores of size 0.8-1.3 nm. Compared with microporous material NPC-0, the mesopores in NPC-c can only derive from the decomposition of surfactant F127 during carbonization process. It indicates that its is possible to prepare
35 mesoporous carbon from PBZs by a soft-templating method. The N_2 sorption isotherms for NPC-1~NPC-3 are very similar, exhibiting no obvious hysteresis loop and slightly increase of nitrogen uptake at high relative pressure (p/p_0 = 0.9-1.0). It implies the absence of mesopores and the existence of few
40 macropores for NPC-1~NPC-3. The N_2 sorption isotherm for NPC-4 reveals a type IV curve with a distinct and wide hysteresis loop in the relative pressure range of 0.45-0.9, demonstrating the existence of disordered mesopore structure.[41] The PSDs of the NPCs are shown in Fig. 3b, whose reliability can be proved by a
45 good fitting between the simulated adsorption isotherms based on the DFT theory assuming the split-shaped pores and the experimental data (Fig. S1†).[42] It can be seen that NPC-1~NPC-3 are composed of abundant micropores in the narrow range of 0.7-1.1 and 1.7-1.9 nm, and few macropores. As the usage of soft-
50 templating agent F127 increased, the micropores were slightly developed and broadened for NPC-1-NPC-4, and more large-sized micropores of size 1.7-1.9 nm were created. During the evaporation of the solvent, the concentration of the triblock copolymer F127 enriched and drives the organization of PBZ-
55 copolymer composites into micelles. The micelles were composed of hydrophobic PPO segments as the cores and surrounded by PEO-PBZ composite shell.[43] With the increase of concentration of block copolymer F127 in the synthetic system, the number of block copolymers in a micelle increased resulting
60 in an enlargement of the size of the micellar aggregates.[44] The micellar aggregates further decomposed to form more large-sized nanostructure during thermal treatment, which leaded to the generation of the larger-sized micropores. Noticeably, the concentration of F127 for the preparation of NPC-1~NPC-3 were
65 not enough to grow into mesostructure by EISA, so it could not produce any mesopores in the resulting carbon materials.[44,45] When the molar ratio of F127 : urea reached 0.020 : 1, the mesostructure occured in the carbonized sample NPC-c. After activation by KOH, the mesopore size was enlarged from the size
70 range of 2.5-2.7 nm for NPC-c to 5.0-6.1 nm for its activated sample NPC-4. The expansion of the mesopore framework could be ascribed to be the etching action between the mesopore walls and the activating agent during KOH activation, which leads to the broadened mesopore walls.[46] As a result, NPC-4 exhibits a
75 hierarchical pore structure: abundant micropores, limited disordered mesopores, and few macropores.

Table 1 Yield and textural characteristics of the NPCs.

Sample	Yield[a] (wt. %)	S_{BET} (m^2 g^{-1})	S_{micro} (m^2 g^{-1})	V_{total} (cm^3 g^{-1})	V_{micro} (cm^3 g^{-1})	V_{micro}/V_{total} (%)
NPC-c	67.9	154.6	89.8	0.15	0.09	58.1
NPC-0	58.4	954.8	857.1	0.45	0.40	88.7
NPC-1	53.3	1097.3	1014.5	0.53	0.47	88.4
NPC-2	49.9	1255.9	1108.4	0.63	0.52	82.4
NPC-3	47.6	1257.8	1059.9	0.65	0.49	75.6
NPC-4	41.3	856.8	792.0	0.53	0.37	69.0

ARTICLE TYPE

^{a} Yield (wt. %) = (dry NPC mass / precursor mass)*100.

The textural properties of the NPCs are listed in Table 1. The mesoporous carbon NPC-c possesses a low BET surface area of 154.6 m^2 g^{-1}, a small pore volume of 0.15 cm^3 g^{-1}, and the
5 lowest micropore fraction of 58.1 % among all NPCs. The activated samples NPC-0~NPC-4 have high specific BET surface area of ranging from 856.8 to 1257.8 m^2 g^{-1}. Compared with its carbonized sample NPC-c, the BET surface area, total / micro-pore volume of NPC-4 greatly increased, showing the
10 effectiveness of activation agent KOH in generation new pores in the carbon network by chemical activation. The redox reaction between carbon and KOH is shown in equation (1).^{47,48}

$$6KOH + 2C \rightarrow 2K + 3H_2 + 2K_2CO_3 \qquad (1)$$

$$K_2CO_3 \rightarrow K_2O + CO_2 \qquad (2)$$

15 $$CO_2 + C \rightarrow 2CO \qquad (3)$$

$$K_2CO_3 + 2C \rightarrow 2K + 3CO \qquad (4)$$

$$K_2O + C \rightarrow 2K + CO \qquad (5)$$
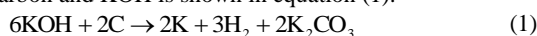
It is noticeable that the precursor can only be activated by KOH at activation temperature below 600 ^{o}C,^{19} as K$_2$CO$_3$ will
20 decompose into K$_2$O and CO$_2$ at temperature over 700 ^{o}C (equation (2)), and then the reduction of as-formed potassium compound (equation (4) and (5)) and carbon dioxide (equation (3)) by carbon will occur. The activation process at 600 ^{o}C introduces additional, abundant micropores into the carbon
25 network for NPC-0~NPC-4. Furthermore, the presence of large-sized micropores in NPC-1~NPC-3, which are derived from the decomposition of the soft-templating agent after carbonization, are beneficial for the homogeneous distribution of KOH aqueous solution inside the pore walls during the impregnation procedure.
30 It further facilitates the redox reactions between carbon and the potassium compound in the pore channels,^{49} which leads to the great increase of micropore area and micropore volume for NCP-1~NPC-3, in comparison with NPC-0 (see Table 1). Therefore, as the usage of surfactant F127 increased from zero to the maximum,
35 the BET surface area, and total pore volume increased evidently for NPC-0~NPC-3, but decreased for NPC-4. The decrease of surface area and pore volume for NCP-4 is probably due to the severe etching action by KOH in the nanostructured carbon skeleton (NPC-c), leading to the formation of widened micro-
40 /mesopore structure for NPC-4, as shown in the PSD curves in Fig. 3b. As a result, the hierarchically porous carbon material NPC-4 shows the lowest surface area, smallest pore volume, and lowest microporosity among the five KOH-activated carbons.
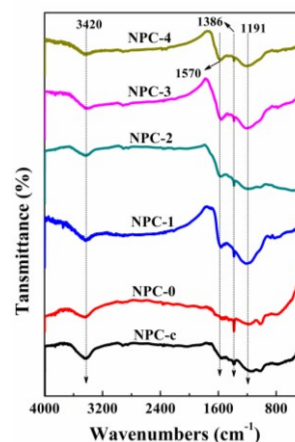
Fig. 4 FT-IR spectra of the NPCs.

The NPCs were characterized by FT-IR spectroscopy (Fig. 4). All spectra of the NPCs show similar broad absorption bands,
50 due to the strong absorption of carbon. The broad band at about 3420 cm^{-1} is assigned to O-H or N-H stretching vibrations. The bands at 1570 cm^{-1} belong to the N-H in-plane vibrations or the stretching vibration of aromatic rings. The peaks at 1386 cm^{-1} represent to C-N stretching vibrations. The broad bands at 1191
55 cm^{-1} correspond to C-N or C-O stretching vibrations. The weak peaks at 900-650 cm^{-1} are assigned to C-H and N-H out-of-plane deformations. These results demonstrate the existence of C-N and N-H species in the NPCs.

The chemical compositions of all NPCs were determined by
60 elemental analysis and the results are illustrated in Table S1†. It reveals that all NPCs possess similar high nitrogen content in the range of 5.21-5.67 wt. %, which can only derive from urea as the nitrogen source. It indicates that the introduction of the soft-templating agent had little influence on the nitrogen content, and
65 the nitrogen species in the carbon network exhibited excellent thermal stability. Compared with NPC-0, both the carbon and nitrogen content for NPC-1~NPC-4 decreased slightly with the increase of the usage of F127. It is probably due to more easily decomposition of N species in the carbon framework in the
70 presence of higher concentration triblock copolymer F127 during the thermal treatment.

XPS analyses is applied to further investigate the nature of the nitrogen functionalities on the surface of the NPCs, as shown in Table S2† and Fig. 5. The N 1s spectrum of all NPCs can be
75 deconvoluted into four peaks with the binding energies centered at 398.5, 400.2, 401.0, and 403 eV, which are assigned to pyridinic nitrogen (N-6), pyrrolic nitrogen or pyridonic nitrogen (N-5), quaternary nitrogen (N-Q) and pyridine-N-oxide (N-X), respectively.^{23,50} N-6 were gradually removed but more N-5 and
80 N-Q formed with increase of usage of surfactant F127 for NPC-0~NPC-4. It implied that under oxidising conditions (including the presence of oxygen-rich triblock copolymer during

carbonization process and activating agent KOH during activation process), N-5 and N-Q were more stable than other nitrogen species.
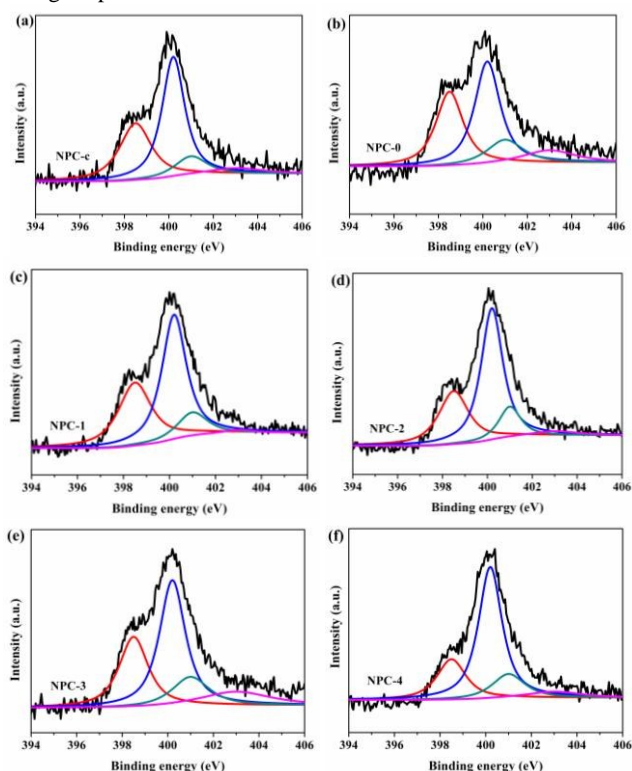
Fig. 5 N1s spectra of (a) NPC-c, (b) NPC-0, (c) NPC-1, (d) NPC-2, (e) NPC-3, and (f) NPC-4.

Furthermore, N-6 were partially converted into N-5 and N-Q. The N-X species, which accounted for 2.39~8.68 at. % of all samples, were probably formed by oxidation under the above mentioned oxidising conditions, or in air due to exposure to the ambient. Such compositions of nitrogen functionalities are very similar to the nitrogen-rich porous carbon materials with high CO_2 capacity that have been reported previously.[51,52,53,54] Consequently, the PBZ-based N-rich porous carbon materials are considered to be ideal candidates for CO_2 capture.
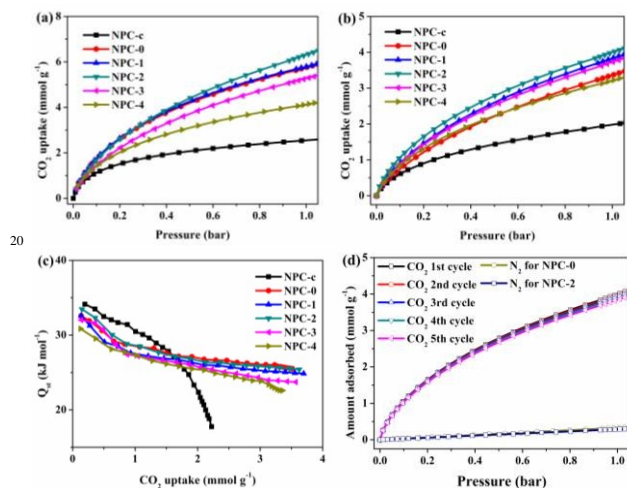
Fig. 6 CO_2 adsorption isotherms at (a) 0 and (b) 25 °C for all samples. (c) Isosteric heat of CO_2 adsorption for the NPCs. (d) CO_2 multi-cycle adsorption isotherms (filled circles) for NPC-2, and N_2 adsorption isotherms (open circles) for NPC-0 and NPC-2 at 25 °C, respectively.

The NPCs were utilized as adsorbents for CO_2 capture to study their CO_2 capture performance. The CO_2 adsorption isotherms of PBZ-based NPCs were measured at 0 (Fig. 6a) and 25°C (Fig. 6b) under atmospheric pressure (1 bar), respectively. The corresponding adsorption uptakes at 1 bar by Autosorb-1 are presented in Table 2. The carbonized sample NPC-c, which possesses low surface area (154.6 m^2 g^{-1}) and low pore volume (0.15 cm^3 g^{-1}), exhibits relatively low CO_2 uptakes of 2.55 and 1.98 mmol g^{-1} at 0 and 25 °C and 1 bar, respectively. However, the CO_2 adsorption uptakes of NPC-c are much higher than commercial activated carbons with high surface area (1150-3450 m^2 g^{-1}) and pore volume (0.43-1.79 cm^3 g^{-1}) under identical conditions (< 2 mmol g^{-1} at 0 °C and 1 bar).[55] It can be attributed to the presence of the high nitrogen content, which can effectively enhance the adsorption capacity of acidic CO_2 gas. At 1 bar, KOH-activated samples NPC-0~NPC-4 display significant CO_2 uptakes of 4.71-6.35 mmol g^{-1} at 0 °C, and 3.25-4.02 mmol g^{-1} at 25 °C, respectively. Such great improvement of the CO_2 uptakes for NPC-0~NPC-4 is mainly ascribed to the well-developed micropore structure by KOH activation, in comparison with the carbonized sample NPC-c. All samples show decreased CO_2 uptakes as the adsorption temperature arises from 0 to 25 °C, which is well agreement with the references.[16, 17, 19, 24]

Table 2 The CO_2 uptakes of the NPCs at 1 bar.

Sample	CO_2 uptake by Autosorb-1 / mmol g^{-1} (wt. %)		CO_2 uptake by TGA / mmol g^{-1} (wt. %)			
			100 % CO_2		15 % CO_2	
	0 °C	25 °C	25 °C	75 °C	25 °C	75 °C
NPC-c	2.55(11.23)	1.98(8.72)	-	-	-	-
NPC-0	5.30(23.33)	3.40(14.96)	3.30(14.54)	1.22(5.37)	1.52(6.67)	0.37(1.62)
NPC-1	5.82(25.61)	3.86(17.01)	3.77(16.59)	1.34(5.90)	1.59(7.01)	0.40(1.77)
NPC-2	6.35(27.95)	4.02(17.70)	3.82(16.80)	1.40(6.14)	1.77(7.81)	0.46(2.03)
NPC-3	5.79(25.50)	3.78(16.65)	3.76(16.54)	1.32(5.82)	1.55(6.83)	0.40(1.76)
NPC-4	4.71(20.76)	3.25(14.30)	3.21(14.11)	1.23(5.43)	1.49(6.55)	0.45(1.96)

Nanoscale Accepted Manuscript

ARTICLE TYPE
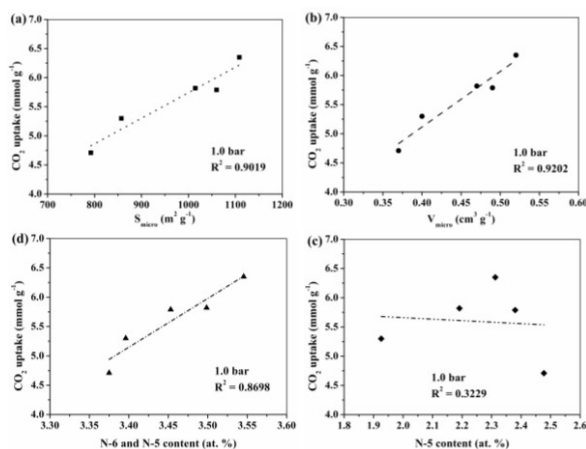
Fig. 7 CO_2 uptake at 1.0 bar (0 °C) versus (a) micropore surface area, (b) micropore volume, (c) N-5 content, and (d) N-6 and N-5 content.

Compared with NPC-0, CO_2 uptakes at 25 °C and 1 bar increased by 13.5, 18.2 and 11.2 % for NPC-1, NPC-2 and NPC-3, respectively, but decreased by 4.4 % for NPC-4. It is well known that the kinetic diameter of single CO_2 molecule is 0.33 nm, and only pore size less than five times that of the molecular size of the adsorbate are effective for gas adsorption at ambient pressure.[38] Therefore, the micropores with pore size smaller than 1.5 nm, which have high adsorption potential, are mainly responsible for CO_2 adsorption at atmospheric or low pressure.[13] Fortunately, the PSDs of KOH-activated samples NPC-0~NPC-3 mainly range from 0.7 to 1.1 nm except for NPC-4 (see Fig. 3b). Comparison with NPC-0, the introduction of surfactant F127

resulted in the increase of the micropore surface and micropore volume for NPC-1~NPC-3. The higher micropore surface area and larger micropore volume offers more CO_2 physical adsorption sites, which accounts for higher CO_2 uptakes for NPC-1~NPC-3 than that of NPC-0. Fig. 7a demonstrates that there is a linear trend between the CO_2 uptake (at 0 °C and 1 bar) and the micropore surface area (correlation coefficient of 0.90). Similarly, the CO_2 uptake also changes linearly with the micropore volume (correlation coefficient of 0.92, Fig. 7b). It reveals that the CO_2 uptakes for NPC-0~NPC-4 are closely associated with their micropore surface area and micropore volume. It can be inferred that micropore volume and micropore surface area of the NPCs are the determining factors in CO_2 capture at ambient pressure.[10,13,54] A loss of CO_2 uptake for NPC-4 can be attributed to a broad PSD with the lowest microporosity among five KOH-activated samples.

Remarkably, the sample NPC-2 displays the maximum CO_2 uptake of 4.02 mmol g^{-1} at 25 °C and 6.35 mmol g^{-1} at 0 °C under 1 bar, respectively (Table 2). It can be ascribed to its high micropore surface area and micropore volume to provide abundant CO_2 adsorption sites, appropriate pore size distribution, and high nitrogen content. Such high CO_2 uptake is comparable to or higher than that of most recently reported nitrogen-doped porous carbon materials as shown in Table 3. It is clear from this comparison that the nitrogen-rich NPCs derived from PBZs, with inexpensive and convenient primary amine as nitrogen source, exhibit high CO_2 uptakes under simple and mild synthesis conditions, which are ideal solid adsorbents for CO_2 capture at ambient pressure.

Table 3 Comparison of CO_2 uptakes and CO_2 / N_2 selectivity at 25 °C and 1 bar for different nitrogen-containing porous carbon materials.

Adsorbents	S_{BET} (m² g⁻¹)	N (wt. %)	CO_2 uptake (mmol g⁻¹)	Normalized CO_2 uptake per S_{BET} (μmol m⁻²)	CO_2 / N_2 selectivity (25 °C, 1.0 bar)	Reference
Microporous carbons	1256	0	4.5	3.58	50	7
Nitrogen enriched porous carbon	490	0.32	2.25	4.59	-	24
Highly porous N-doped carbon monoliths	1740	3.38	4.57	2.63	29	56
Nanostructured templated carbon	2559	7.0	4.0	1.56	14	57
Chitosan derived nitrogen-doped microporous carbons	1381	4.59	3.9	2.82	21	51
Nitrogen-containing microporous carbon spheres	809	2.0	4.0	4.94	-	13
N-doped mesoporous carbon from IBN-9	1181	12.91	4.5	3.81	32	53
N-doped carbon from polypyrrole	1700	10.14	3.9	2.29	5.3	54
NPC-2 derived from polybenzoxazine	1255.9	5.25	4.02	3.20	32.4	This work

Nanoscale Accepted Manuscript

ARTICLE TYPE
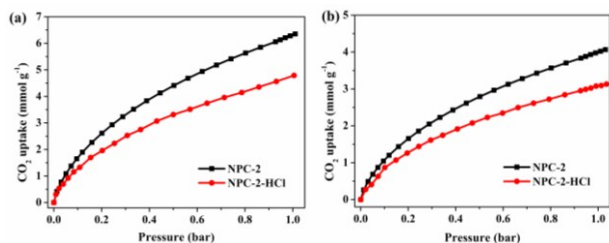
Fig. 8 CO_2 adsorption isotherms of NPC-2 and NPC-2-HCl at (a) 0 and (b) 25 °C, respectively.

Except for the textural properties, the surface functionality of carbonaceous materials also have influence on the CO_2 capture at atmospheric pressure. The N atom (Lewis base), possessing a pair of lone electrons, can enhance the affinity by strong pole-pole interactions between the N-doped surface of carbon and the acidic CO_2 molecules, and act as an anchor for CO_2 capture.[6,9,51,54] To prove the enhancement of the CO_2 adsorption uptake by the incorporation of basic nitrogen species, the NPC-2 was firstly neutralized by concentrated HCl and then the CO_2 adsorption isotherms of the NPC-2-HCl was measured at 0 and 25 °C, respectively. The XPS survey spectra (Fig. S2a†) reveals the existence of Cl (3.06 at. %) and N (4.05 at. %) in NPC-2-HCl, while none Cl and N (4.24 at. %) in NPC-2. It suggests that HCl treatment leads to the incorporation of Cl into the carbon, but have little influence on the nitrogen content (see Table S3†). As shown in Fig. S2b†, the N 1s signal reflects the change of the nitrogen species before and after HCl treatment. In detail, the binding energy of pyridinic nitrogen (N-6) shifts from 398.5 eV for NPC-2 to 398.3 eV for NPC-2-HCl, while pyrrolic nitrogen or pyridonic nitrogen (N-5) shifts from 400.2 eV for NPC-2 to 399.8 eV for NPC-2-HCl. It implies that Cl ions might be adsorbed into the narrow pores and chemically bonded to the surface basic nitrogen functional groups (N-6 and N-5).[30,58] Moreover, a very similar porosity (slight smaller surface area and pore volume than that of NPC-2, as well as similar PSD) has been observed for sample NPC-2-HCl (see Fig. S3† and Table S4†). In a word, concentrated HCl treatment has little effect on the textural properties of NPC-2. As shown in Fig. 8a and 8b, the CO_2 uptakes at 1.0 bar for NPC-2-HCl were measured to be 4.78 and 3.08 mmol g^{-1} at 0 and 25 °C, respectively, which are much lower than that of NPC-2 (6.35 and 4.02 mmol g^{-1} at 0 and 25 °C under 1 bar, respectively). It clearly exhibits that acid treatment leads to a 21~25 % CO_2 uptake loss of the total CO_2 uptakes. In order to better understand the CO_2 adsorption performance of the NPCs without the influence of surface area, CO_2 adsorption capacities were normalized with respect to total surface area. After normalized by surface area, CO_2 uptakes per m^2 (μmol m^{-2}) at 0 °C and 1.0 bar for NPC-2 and NPC-2-HCl were 5.06 and 4.09 μmol m^{-2}, respectively. These values are higher than those of many reported porous carbon materials (see Table 3). Based on

the similar textural properties for NPC-2 and NPC-2-HCl, it can be inferred that the evident decrease of CO_2 uptake for NPC-2-HCl can be only ascribed to the loss of large number of basic nitrogen functionalities after neutralization by acid. From this comparison, it demonstrates that the presence of basic nitrogen functionalities in the carbon surface make great contribution to the enhancement of the CO_2 adsorption capacities.

Furthermore, to estimate the difference of the strength of the interaction between CO_2 molecules and NPC-2 as well as NPC-2-HCl, their isosteric heats of adsorption (Q_{st}) (Fig. S4†) were determined from the CO_2 adsorption isotherms measured at 0 and 25 °C using the Clausius-Clapeyron equation. The isosteric heats of adsorption of CO_2 on NPC-2 lie in the range 25.4-33.5 kJ mol^{-1} with the CO_2 uptakes varying from 0.1 to 3.6 mmol g^{-1}, while decrease to 11.8-20.1 kJ mol^{-1} for NPC-2-HCl with the CO_2 uptakes varying from 0.1 to 3.0 mmol g^{-1}. It has been reported that the isosteric heat of adsorption of CO_2 for carbonaceous materials (especially for non-polar adsorbents) lies in the range of 16~25 kJ mol^{-1}.[55,59] Thus, it can be concluded that the nature of the adsorption of CO_2 by NPC-2-HCl is physical adsorption which mainly depends on its micropore structure.[55] In addition, in contrast to NPC-2, low Q_{st} value for NPC-2-HCl can be attributed to the loss of basic groups for NPC-2-HCl after neutralization treatment and the presence of acidic HCl attached to the carbon surface. However, two adsorption mechanisms coexists in NPC-2, including the strong acid-base interactions between the basic nitrogen functionalities and acidic CO_2 molecules, as well as physical adsorption in the fine micropores.[60,61] As a result, the Q_{st} value for NPC-2 is much higher than that of NPC-2-HCl, which further confirms that the importance of basic nitrogen functionalies in the carbon network for high-performance CO_2 capture.

It has been widely reported that pyrrolic nitrogen (N-5) make significant contribution to the CO_2 capture, but other types nitrogen functionalities have little contribution to the CO_2 capture.[30,32] In order to distinguish which types of basic nitrogen functionalities are effective for acidic CO_2 adsorption, the N-5 content as well as N-6 and N-5 contents of the NPCs is correlated with the amount of CO_2 adsorbed at 0 °C and 1.0 bar. Fig. 7c shows that there is no clear trend correlating the CO_2 uptake and N-5 content, indicating the presence of N-5 does not govern the CO_2 adsorption performance of the NPCs. However, there is a clear trend correlating the CO_2 uptake and N-6 and N-5 contents of the NPCs, resulting in a much higher correlation coefficient of 0.87 than that of N-5 content correlating with the CO_2 uptake (correlation coefficient of 0.32). It indicates that both N-5 and N-6 contents might have an important influence on the CO_2 sorption behavior, which is consistent with the results obtained from the the neutralization of the basic nitrogen species experiment. Based on generalized Lewis acid-base theory, as to N-6, which neighbours two carbon atoms in a graphitic sp^2 network, displays the strong hydrogen bond interactions with the surrounding C-H bonds.[50] As to pyridonic-N, the p orbital in its -OH can produce

ARTICLE TYPE

p-π conjunction effect with its π bond, resulting in the enhancement of its Lewis basicity.[38,45,51] Therefore, N-6 and pyridonic-N in N-5 exhibit stronger Lewis basicity than other types of nitrogen functionalities, which are effective Lewis-base
5 sites for binding the acidic CO_2 and improve the CO_2 adsorption capacity.[52] Fortunately, N-5 and N-6 are the main nitrogen forms (more than 77.9 at. % of the total N content) for all NPCs. Remarkably, N-6 and N-5 account for 3.77, 3.40, 3.64, 3.54, 3.45, and 3.37 at. % of their corresponding total nitrogen contents for
10 NPC-c~NPC-4, respectively (calculated from the XPS data in Table S1† and Table S2†). Consequently, NPC-1~NPC-3, with higher contents of N-6 and N-5, display higher CO_2 uptakes than that of NPC-0. It should be pointed out that larger micropore surface area and micropore volume for NPC-1~NPC-3 than that
15 of NPC-0 also account for their high CO_2 uptakes. Although NPC-c possesses the highest N-6 and N-5 contents among the six samples, it shows the lowest CO_2 uptakes at 0 and 25 ^{o}C, 1 bar (see Table 2), due to its lowest microporosity. It further implies that micropore structure plays a more important role in CO_2
20 capture at amibent pressures. In addition, the lowest CO_2 uptakes for NPC-4 under the same adsorption conditions among the five KOH-activated samples also partially result from its lowest N-6 and N-5 content. Thus, it can be inferred that CO_2 capture at amibent or low pressures by porous carbon-based adsorbents
25 strongly depends on the micropore structure (including micropore surface area, micropore volume, pore dimension and PSD of micropore) as well as surface nitrogen functionalities in the carbon network.

The isosteric heats of CO_2 adsorption (Q_{st}) for all NPCs were
30 also calculated using CO_2 adsorption isotherms at 0 and 25°C based on Clausius-Claperon equation (Fig. 6c). The Q_{st} values for all samples are exhibited in Fig. 6c. The isosteric heat of adsorption of CO_2 on all samples lies in the range 17-35 kJ mol^{-1} with the CO_2 uptakes varying from 0.1 to 3.8 mmol g^{-1}, which are
35 higher than those previously reported for various nitrogen-containing porous carbons.[25,38,62] Such high isosteric heat can be attributed to the strong acid-base interaction between basic nitrogen functionalities and acidic CO_2 molecules. It is remarkable that the initial isosteric heat of adsorption for NPC-c
40 with the highest nitrogen content among all samples is higher than that of NPC-0~NPC-4 with slightly lower nitrogen contents at low CO_2 uptakes. It confirms that the importance of the presence of nitrogen functionalities in enhancing the CO_2 uptake. As the CO_2 uptakes exceeded 2.0 mmol g^{-1}, the Q_{st} values for
45 NPC-c decreased significantly to 17-22 kJ mol^{-1}, indicating the weak interaction between CO_2 and the carbon host. The decrease of the Q_{st} values at higher CO_2 uptake could be attributed to the fewer accessible, unoccupied sites for the CO_2 adsorption at a higher CO_2 uptake. But even at a high coverage (3.3 mmol g^{-1}),
50 other five KOH-activated samples NPC-0~NPC-4 still retained high Q_{st} values, about 25.8, 25.1, 25.6, 23.8, and 22.6 kJ mol^{-1}, respectively. It can be ascribed to their well-developed micropore structure, in comparison with NPC-c.

In order to investigate the CO_2/N_2 selectivity of the NPCs,
55 the N_2 adsorption capacity is also tested under the same experimental conditions. Fig. 6d shows the N_2 adsorption isotherms at 25 ^{o}C of NPC-0 and NPC-2. It can be seen that the uptakes of N_2 mmol g^{-1} at 25 ^{o}C and 1 bar for NPC-0 and NPC-2 are 0.32 and 0.28 mmol g^{-1}, respectively, which are much lower
60 than their corresponding CO_2 uptakes. The IAST of Myers and Prausnitz is well-known to predict the binary gas mixture adsorption on many porous adsorbent materials.[63,64] The adsorption selectivity (S_{ads}) for binary mixtures of CO_2 and N_2 is defined as follows:[63,65]

$$S_{ads} = \frac{q_1/q_2}{p_1/p_2}$$

where q_i is the amount of i adsorbed and p_i is the partial pressure of i in the mixture.

Fig. S5† presents the predicted CO_2/N_2 selectivities as a function of CO_2 molar fraction with the overall pressure of 1.0
70 bar for NPC-0 and NPC-2. It can be found that the calculated CO_2/N_2 adsorption selectivities decrease with the increase of CO_2 molar fraction for both NPC-0 and NPC-2. The sample NPC-2 exhibits much higher CO_2/N_2 adsorption selectivities (26.4-41.3) than that of NPC-0 (18.0-28.8) over the entire range. When
75 evaluating any post-combustion CO_2 capture materials for CO_2/N_2 separation application, it is essential to determine their selectivity factors. Thus, it is prevalent to calculate the adsorption selectivitis for a mixture of approximately 0.15 bar CO_2 and 0.75 bar N_2 at 25 ^{o}C. At the total pressure of 1.0 bar and CO_2
80 concentration of 15 % (partial pressure of 0.15 bar), the CO_2/N_2 adsorption selectivities for NPC-0 and NPC-2 are calculated to be 22.3 and 32.4 by IAST, respectively. It indicates that such NPCs have high selectivity for CO_2/N_2 separation. The selectivity of NPC-2 is comparable to, or even higher than those previously
85 reported values as listed in Table 3. Compared with NPC-0, the enhancement of the selectivity of NPC-2 for CO_2 over N_2 is probably due to its more developed micropore structure, appropriate PSD, and slightly higher N-6 and N-5 content.
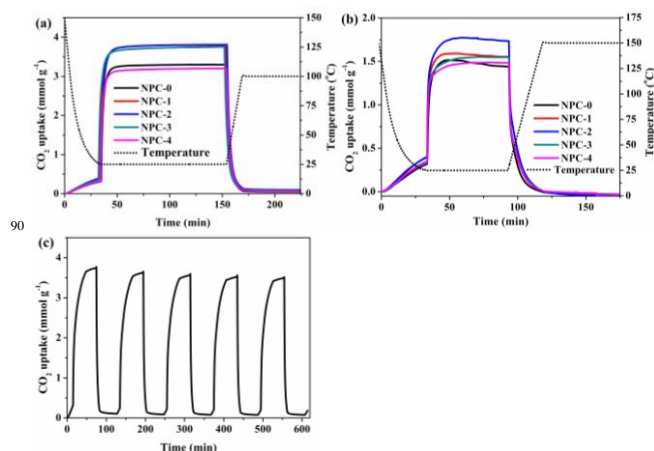
Fig. 9 TGA records of CO_2 uptakes of the KOH-activated samples NPC-0~NPC-4 at 25 ^{o}C and 1 bar (a) in 100% CO_2, (b) in 15 vol% CO_2 and 85 vol% N_2 gas flow. (c) 100% CO_2
95 adsorption - desorption cycles obtained for NPC-2.

To evaluate the CO_2 adsorption/desorption dynamics

property, regenerability and stability of the NPCs, their CO_2 capture performance were further investigated by a TGA analysis. Fig. 9a exhibits the adsorption / desorption kinetics of pure CO_2 for NPC-0~NPC-4 at 25 °C and 1 bar by TGA. A sharp weight gain was observed after they were exposed to pure CO_2 in the first 5 min. More than 93 % of the pure CO_2 were adsorbed within 10 min, and approximately 60 min was needed to attain 99 % of the maximum adsorption capacities for NPC-0~NPC-4. It also can be seen that the adsorbed CO_2 were quickly desorbed within 30 min when the CO_2 gas was changed to N_2 and the temperature increased to 100 °C. Fig. 9b further shows the adsorption / desorption kinetics under simulated flue gas conditions (15 vol. % CO_2 and 85 vol. % N_2) for all samples at 25 °C and 1 bar by TGA. Similarly, exceeding 92 % of the dilute CO_2 were adsorbed within 10 min, and 60 min were enough to attain 97 % of the maximum adsorption capacities for NPC-0~NPC-4, also exhibiting very high adsorption rate. The adsorbed CO_2 could be quickly desorbed within 30 min at 150 °C under a N_2 flow. The phenomenon can be attributed to the existence of abundant micropores, appropriate PSDs as well as basic nitrogen functionalities for NPC-1~NPC-4, which lead to high adsorption potentials and enhanced affinity for CO_2[5,6,7]. In a word, such well-developed micropore structure and appropriate pore structure of the PBZ-based NPCs ensures a fast adsorption/desorption rare and short regeneration time. The CO_2 capture performance was also investigated by TGA at 75 °C and the results are listed in Table 2. As the adsorption temperature increased from 25 to 75 °C, the adsorption capacities of pure CO_2 for NPC0~NPC-4 decreased evidently from 3.30-3.82 mmol g^{-1} at 25 °C to 1.22-1.40 mmol g^{-1} at 75°C under 1 bar. It indicates that CO_2 adsorption by the NPCs is an exothermic process[44,53]. Similarly, the adsorption capacities of 15 % CO_2 dropped from 1.49-1.77 mmol g^{-1} at 25 °C to 0.37-0.46 mmol g^{-1} at 75 °C under 1 bar with the increase of adsorption temperature. It further reveals that the NPCs have a high selectivity of CO_2 over N_2 because of the presence of large number of basic N-6 and N-5 functionalities.

Cyclic adsorption / desorption of CO_2 for NPC-2 exhibits no noticeable decrease after 5 cycles in the isotherms by Autosorb-1 (Fig. 6d) and in the CO_2 adsorption / desorption kinetics by TGA (Fig. 9c), respectively. The sample NPC-2 can be easily and quickly regenerated with negligible loss of CO_2 uptake, indicating superior recyclable stability for CO_2 capture. Such excellent capture performance is due to its well-developed microporosity, appropriate pore size distribution, and abundant nitrogen functional groups.

Conclusions

A series of novel nitrogen-rich porous carbons derived from bifunctional polybenzoxazine were successfully synthesized by a soft-templating method together with KOH chemical activation method. The pore structure of the nitrogen-rich porous carbons can be easily tailored by changing the concentration of the soft-templating agent F127. Low concentration of the soft-templating agent resulted in the development of the microporosity, but high concentration leaded to the hierarchical pore structure with low microporosity, and poor CO_2 capture performance. Both the micropore structure and surface chemistry of nitrogen-rich carbons have an significant influence on CO_2 adsorption properties. At 1 bar, the CO_2 adsorption capacity for material NPC-2 can reach 4.02 and 6.35 mmol g^{-1} at 25 and 0 °C, respectively. The NPCs also show a good selectivity for CO_2/N_2 separation, high adsorption/desorption rate and they can be easily regenerated. The CO_2 capture performance reveals that such polybenzoxazine based nitrogen-rich porous carbons are potentially excellent CO_2 adsorbents.

Acknowledgments

Notes and references

[a] Institute of Coal Chemistry, Chinese Academy of Sciences, Taiyuan 030001, P. R. China. Fax: 86 351 4250292; Tel: 86 351 4250292; E-mail: likx@sxicc.ac.cn
[b] Graduate University of Chinese Academy of Sciences, Beijing 100049, P. R. China

† Electronic Supplementary Information (ESI) available: Elemental and XPS analysis and XPS peak positions and relative content of N species in the NPCs. See DOI: 10.1039/b000000x/

1   K. N. Wood, R. O'Hayre and S. Pylypenko, *Energy Environ., Sci.*, 2014, **7**, 1212.
2   B. E. Gurkan, J. C. de la Fuente, E. M. Mindrup, L. E. Ficke, B. F. Goodrich, E. A. Price, W. F. Schneider and J. F. Brennecke, *J. Am. Chem. Soc.*, 2010, **132**, 2116.
3   S. R. Venna and M. A. Carreon, *J. Am. Chem. Soc.*, 2010, **132**, 76.
4   S. Choi, M. M. L. Gray, C. W. Jones, *ChemSusChem*, 2011, **4**, 628.
5   G. T. Rochelle, *Science*, 2009, **325**, 1652.
6   A. B. Rao and E. S. Rubin, *Environ. Sci. Technol.*, 2002, **36**, 4467.
7   B. Adeniran, E. Masika and R. Mokaya, *J. Mater. Chem. A*, 2014, **2**, 14696.
8   R. Li, X. Ren, X. Feng, X. Li, C. Hu and B. Wang, *Chem. Commun.*, 2014, **50**, 6894.
9   J. Zhou, W. Li, Z. Zhang, W. Xing and S. Zhuo, *RSC Advances*, 2012, **2**, 161.
10 M. Sevilla, J. B. Parra and A. B. Fuertes, *ACS Appl. Mater. Interfaces*, 2013, **5**, 6360.
11 R. L. Liu, W. J. Ji, T. He, Z. Q. Zhang, J. Zhang and F. Q. Dang, *Carbon*, 2014, **76**, 84.
12 M. Nandi, K. Okada, A. Dutta, A. Bhaumik, J. Maruyama, D. Derks and H. Uyama, *Chem. Commun.*, 2012, **48**, 10283.
13 L. Liu, Q. F. Deng, X. X. Hou and Z. Y. Yuan, *J. Mater. Chem.*, 2012, **22**, 15540.
14 A. Houshmand, W. M. A. W. Daud and M. S. Shasfeeyan, *Separ. Sci. Technol.*, 2011,**46**, 1098.
15 C. Pevida, M. G. Plaza, B. Arias, J. Fermoso, F. Rubiera and J. J. Pis, *Appl. Surf. Sci.*, 2008, **254**, 7165.
16 A. Houshmand, W. M. A. W. Daud, M. G. Lee and M. S. Shafeeyan, *Water Air Soil Poll.*, 2012, **223**, 827.
17 A. Arenillas, K. M. Smith and T. C. Drage, *Fuel*, 2005, **84**, 2204.
18 M. Abe, K. Kawashima, K. Kozawa, H. Sakai and K. Kaneko, *Langmuir*, 2000, **16**, 5059.
19 Z. X. Wu, P. A. Webley and D. Y. Zhao, *J. Mater. Chem.*, 2012, **22**, 11379.
20 C. L. Mangun, K. R. Benak, J. Economy and K. L. Foster, *Carbon*, 2001, **39**, 1809.
21 P. Vinke, M. van der Eijk, M. Verbree, A. F. Voskamp and

Journal Name

Nanoscale

ARTICLE TYPE

H. van Bekkum, *Carbon*, 1994, **32**, 675.

22 S. Biniak, G. Szymanski, J. Siedlewski and A. Swiatkoski, *Carbon*, 1997, **35**, 1799.

23 A. H. Lu and J. T. Zheng, *Carbon*, 2002, **40**, 1353.

24 C. Pevida, T. C. Drage and C. E. Snape, *Carbon*, 2008, **46**, 1464.

25 J. C. Wang and Q. Liu, *Nanosacle*, 2014, **6**, 4148.

26 L. Zhao, N. Baccile, S. Gross, Y. J. Zhang, W. Wei, Y. H. Sun, M. Antonietti and M. M. Titirici, *Carbon*, 2010, **48**, 3778.

27 A. S. Gonzalez, M. G. Plaza, F. Rubiera and C. Pevia, *Chem. Eng. J.*, 2013, **230**, 456.

28 J. A. Thote, K. S. Iyer, R. Chatti, N. K. Labhsetwar, R. B. Biniwale and S. S. Rayalu, *Carbon*, 2010, **48**, 396.

29 W. H. Peng, S. M. Zhu, W. L. Wang, W. Zhang, J. J. Gu, D. Zhang and Z. X. Chen, *Adv. Funct. Mater.*, 2012, **22**, 2072.

30 G. P. Hao, W. C. Li, D. Qian, A. H. Lu, *Adv. Mater.*, 2010, **22**, 853.

31 M. Baqar, T. Agag, R. Huang, J. Maia, S. Qutubuddin and H. Ishida, *Macromolecules*, 2012, **45**, 8119.

32 X. Y. Ma, M. H. Cao and C. W. Hu, *J. Mater. Chem. A*, 2013, **1**, 913.

33 M. Florent, M. Tocci and T. J. Bandosz, *Carbon*, 2013, **63**, 283.

34 Y. Yagci, B. Kiskan and N. N. Ghosh, *J. Polym. Sci. Part A: Polym. Chem.*, 2009, **47**, 5565.

35 N. N. Ghosh, B. Kiskan and Yagci, Y. *Prog. Polym. Sci.*, 2007, **32**, 1344.

36 X. Liu and Y. Gu, *J. Appl. Polym. Sci.*, 2002, **84**, 1107.

37 T. Agag, C. R. Arza, F. H. J. Maurer and H. Ishida, *Macromolecules*, 2010, **43**, 2748.

38 G. P. Hao, W. C. Li, D. Qian, G. H. Wang, W. P. Zhang, T. Zhang, A. Q. Wang, F. Schüth, H. J. Bongard and A. H. Lu, *J. Am. Chem. Soc.*, 2011, **133**, 11378.

39 Y. Meng, D. Gu, F. Zhang, Y. Shi, L. Cheng, D. Feng, Z. Wu, Z. Chen, Y. Wan, A. Stein and D. Zhao, *Chem. Mater.*, 2006, **18**, 4447.

40 L. Jin, T. Agag and H. Ishida, *Eur. Polym. J.*, 2010, **46**, 354.

41 M. S. Park, B. O. Jeong, T. J. Kim, S. Kim, K. J. Kim, J. S. Yu, Y. Jung and Y. J. Kim, *Carbon*, 2014, **68**, 265.

42 G. P. Hao, G. Mondin, Z. Zheng, T. Biemelt, S. Klosz, R. Schubel, A. Eychmüller and S. Kaske, *Angew. Chem. Int. Ed.*, 2014, **53**, 1.

43 J. Wei, D. Zhou, Z. Sun, Y. Deng, Y. Xia and D. Zhao, *Adv. Funct. Mater.*, 2013, **23**, 2322.

44 Stephan Förster and Markus Antonietti, *Adv. Mater.*, 1998, **10**, 195.

45 B. Chu. *Langmuir*, 1995, **11**, 414.

46 Y. Lv, F. Zhang, Y. Dou, Y. Zhai, J. Wang, H. Liu, Y. Xia, B. Tu and D. Zhao, *J. Mater. Chem.*, 2012, **22**, 93.

47 E. Raymundo-Pinero, P. Azais, T. Cacciaguerra, D. CazorlaAmoros, A. Linares-Solano and F. Beguin, *Carbon*, 2005, **43**, 786.

48 J. C. Wang and S. Kaskel. *J. Mater. Chem.*, 2012, **22**, 23710.

49 L. K. C. de Souza, N. P. Wickramaratne, Ello, A. S. Ello, M. J. F. Costa, C. E. F. da Costa and M. Jaroniec, *Carbon*, 2013, **65**, 334.

50 W. Wei, C. Liu, Z. Y. Zhao, L. Zhang, J. Zhou, S. P. Zhuo, Z. F. Yan, H. Cao, G. Q. Wang and S. Z. Qiao, *Energy Environ. Sci.*, 2012, **5**, 7323.

51 X. Q. Fan, L. X. Zhang, G. B. Zhang, Z. Shu and J. L. Shi, *Carbon*, 2013, **61**, 423.

52 S. Wang, W. C. Li, L. Zhang, Z. Y. Jin and A. H. Lu, *J. Mater. Chem. A*, 2014, **2**, 4406.

53 Y. F. Zhao, L. Zhao, K. X. Yao, Y. Yang, Q. Zhang and Y. Han, *J. Mater. Chem.*, 2012, **22**, 19726.

54 M. Sevilla, P. V. Vigon and A. B. Fuertes, *Adv. Funct. Mater.*, 2011, **21**, 2781.

55 S. Himeno, T. Komatsu, S. Fujita. *J. Chem. Eng. Data*, 2005, **50**, 369.

56 X. Ma, L. Yao, M. Cao and C. Hu, *J. Mater. Chem.*, 2014, **2**, 4819.

57 L. Wang and R. T. Yang, *J. Phys. Chem. C*, 2012, **116**, 1099.

58 E. Papirer, R. Lacroix, J. B. Donnet, G. Nanse, P. Fioux. *Carbon*, 1995, **33**, 63-72.

59 M. G. Plaza, A. S. Gonzálea, J. J. Pis, F. Rubiera, C. Pevida. *Appl. Energ.*, 2014, **114**, 551.

60 N. P. Wickramaratne, J. Xu, M. Wang, L. Zhu, L. Dai and M. Jaroniec, *Chem. Mater.*, 2014, **26**, 2820-2828.

61 J. Wang, I. Senkovska, M. Oschatz, M. R. Lohe, L. Borchardt. A. Heerwig, Q. Dan, Q. Liu and S. Kaskel, *ACS Appl. Mater. Interfaces*, 2013, **5**, 3160.

62 D. Lee, C. Y. Zhang, C. Wei, B. L. Ashfeld and H. F. Gao, *J. Mater. Chem. A*, 2013, **1**, 14862.

63 A. L. Myers and J. M. Prausnitz, *AIChE J.*, 1965, **11**, 121-127.

64 W. Lu, D. Yuan, J. Sculley, D. Zhao, R. Krishna and H. C. Zhou, *J. Am. Chem. Soc.*, 2011, **133**, 18126.

65 W. G. Lu, J. P. Sculley, D. Q. Yuan, R. Krishna, Z. W. Wei and H. C. Zhou, *Angew. Chem. Int. Ed.*, 2012, **51**, 7480-7484.

Nanoscale Accepted Manuscript